ADVANCED ELECTRONIC MATERIALS Open Access
www.advelectronicmat.de

Epitaxy-Driven Ferroelectric/Non-Ferroelectric Polymorph Selection in an All-Fluorite System

*Eduardo Barriuso, Ricardo Jiménez, Eric Langenberg, Panagiotis Koutsogiannis, Ángel Larrea, Manuel Varela, César Magén, Pedro A. Algarabel, Miguel Algueró, and José A. Pardo**

Films of ferroelectric hafnia have hitherto been deposited on electrodes with a non-fluorite crystal structure. As a result, they are polycrystalline, contain fractions of non-ferroelectric polymorphs or have poor crystal quality. Here, a strategy that circumvents all these limitations is shown. Seven nanometers-thick epitaxial $Hf_{0.5}Zr_{0.5}O_2$ (HZO) films are deposited directly on yttria-stabilized zirconia (YSZ) single-crystals. The fluorite structure of the whole system enables coherent epitaxy, while the substrate orientation induces polymorph-selective growth, being the HZO films orthorhombic on YSZ(111) and monoclinic on YSZ(001). Besides, the YSZ substrate can play the role of a buried floating electrode under the appropriate measuring conditions (temperature and frequency) thanks to its thermally-activated oxygen conductivity. Indeed, out-of-plane ferroelectric switching is confirmed in the orthorhombic HZO samples at 185 °C and 0.01 Hz frequency. This original approach avoids the need to deposit conducting bottom layers, allowing high-quality orthorhombic hafnia to be obtained directly on the substrate and its ferroelectric nature to be studied. Moreover, it constitutes a case of ion-driven ferroelectric switching, and thus gives support to the recently proposed relationship between ionic conductivity, and ferroelectricity in fluorite systems.

1. Introduction

Ferroelectricity arouses great scientific interest from both the fundamental and applied point of view owing to its applications in capacitors, sensors, actuators, energy-efficient devices, and information storage.[1–4] Some of the most widely used ferroelectric materials, such as $BaTiO_3$ and $Pb(Zr,Ti)O_3$, have relatively complex compositions and crystal structures. For this reason, the unexpected discovery of ferroelectricity in thin films of a simple oxide as Si-doped hafnia (HfO_2)[5] opened the door to a frantic research activity since 2011, with thousands of publications reporting on this property in thin films of different HfO_2-based compounds, being the HfO_2-ZrO_2 solid solution the most widely studied system.[6–8]

Bulk HfO_2 and ZrO_2 are isomorphic and mutually soluble. In equilibrium at room temperature and pressure, they show a distorted fluorite crystal structure with monoclinic symmetry (space group $P2_1/c$), but tetragonal $P4_2/nmc$ and cubic $Fm\text{-}3m$ polymorphs are stable in different conditions.[9–11] The formation of solid solutions between HfO_2 or ZrO_2 and other oxides allows the stabilization of selected polymorphs at ambient conditions. For instance, doping ZrO_2 with yttria (Y_2O_3) enables the cubic $Fm\text{-}3m$ structure to be stable up to high temperature for a wide range of Y_2O_3 concentration values, and it is known as yttria-stabilized

E. Barriuso, P. Koutsogiannis, Á. Larrea, C. Magén, P. A. Algarabel, J. A. Pardo
Instituto de Nanociencia y Materiales de Aragón
Universidad de Zaragoza-CSIC
Zaragoza 50018, Spain
E-mail: jpardo@unizar.es

The ORCID identification number(s) for the author(s) of this article can be found under https://doi.org/10.1002/aelm.202300522

DOI: 10.1002/aelm.202300522

E. Barriuso, J. A. Pardo
Departamento de Ciencia y Tecnología de Materiales y Fluidos
Universidad de Zaragoza
Zaragoza 50018, Spain

R. Jiménez, M. Algueró
Instituto de Ciencia de Materiales de Madrid
CSIC
Cantoblanco, Madrid 28049, Spain

E. Langenberg
Departament de Física de la Matèria Condensada
Universitat de Barcelona
Barcelona 08028, Spain

E. Langenberg, M. Varela
Institut de Nanociència i Nanotecnologia de la Universitat de Barcelona (IN2UB)
Universitat de Barcelona
Barcelona 08028, Spain

zirconia (or YSZ). Regarding ferroelectric hafnia, it is an out-of-equilibrium phase belonging to the non-centrosymmetric, orthorhombic $Pca2_1$ space group,[12] although other ferroelectric structures with rhombohedral symmetry ($R3$ or $R3m$ space group) have also been observed in $Hf_{0.5}Zr_{0.5}O_2$[13] and ZrO_2[14,15] films. The unit cell of any of these HfO_2 or ZrO_2 polymorphs can be visualized as a distorted cube with lattice parameters in the range of 5.0 to 5.3 Å.

The deposition of thin films on single-crystalline substrates having a crystal structure similar to that of the material being deposited allows the growth of single-crystal or highly textured layers to be obtained, which facilitates the study of its intrinsic properties minimizing the effects of low-angle grain boundaries. Besides, such epitaxial growth is a useful tool to prepare metastable phases of polymorphic systems as a result of epitaxial stabilization,[16] and is thus the ideal playground for the study of thin films of hafnia and zirconia. Their different polymorphs are very close in energy, and thus tiny mechanical perturbations can tip the balance in favor of a particular one.[10,11,17] Furthermore, in the general case of ferroelectric oxides the strain induced by the substrate on the epitaxial films is well known to provide an additional degree of control over their properties.[18]

Two recent reviews of the literature on hafnia-based epitaxial films,[19,20] reveal that most studies have used substrates with the cubic perovskite structure and lattice constant between 3.85 and 3.95 Å. A bottom electrode, often orthorhombic $(La,Sr)MnO_3$, was deposited before the hafnia film when electrical measurements in the out-of-plane direction were anticipated to study ferroelectricity. Alternatively, some films were grown directly on Nb-doped $SrTiO_3$ conducting substrates, as done for ZrO_2.[14] In these fluorite systems, tensile epitaxial strain is believed to induce the stabilization of the orthorhombic polymorph,[21,22] while compressive stress favors the rhombohedral one.[13–15,23] Just a few studies have explored substrates with non-perovskite structures. For instance, Bégon-Lours et al.[24] reported on the epitaxial growth of strained films of rhombohedral $Hf_{0.5}Zr_{0.5}O_2$ on GaN(0001)-buffered Si(111) substrates.

Of particular interest for the growth of ferroelectric HfO_2 and ZrO_2 is the use of cubic-fluorite YSZ substrates. A major obstacle here is finding a material that could act as a conducting buffer layer between the substrate and the film with a similar crystal structure. Indeed, the first publication on epitaxial hafnia in 2015,[25] used YSZ substrates, but no direct evidence of ferroelectric behavior was given, due to the lack of a bottom electrode. In that case, the orthorhombic structure of the as-grown Y-doped HfO_2 films was demonstrated from crystallographic arguments. Li et al.[26] prepared epitaxial ferroelectric $Hf_{0.5}Zr_{0.5}O_2$ on YSZ with a TiN bottom electrode, but in this case, interface reactions produced TiO_2 layers and poor crystal quality of the hafnia films. Another study reported on the deposition of epitaxial $Hf_{0.5}Zr_{0.5}O_2$ on YSZ(001) using buffer layers of conducting $Pb_2Ir_2O_7$,[27] which has the cubic pyrochlore structure with 10.17 Å bulk lattice constant. The coherent growth of the films on Pb_2Ir_2O was demonstrated by X-ray diffraction from a synchrotron source and transmission electron microscopy, and their polar nature was confirmed through piezoelectric measurements.

Nonetheless, the main research activity on the growth of epitaxial hafnia on YSZ substrates has been led by Funakubo's laboratory, which has explored several crystal orientations and film compositions. These authors reported in 2016 on the ferroelectric switching of oxygen-deficient Y-doped HfO_2 films deposited on (110)-oriented YSZ substrates with indium–tin oxide (ITO) bottom electrodes.[28] ITO (Sn-doped In_2O_3) has the bixbyite structure with a cubic lattice parameter of 10.12 Å, close to twice those of the hafnia polymorphs and YSZ (≈5.15 Å), and thus it can potentially match their fluorite structure. In the case of YSZ(111), the films studied were $Hf_{1-x}Zr_xO_2$,[26,29] Y-doped HfO_2,[30–36] Y-doped $Hf_{1-x}Zr_xO_2$,[37,38] and Ce-doped HfO_2,[39] being TiN the buffer layer in only one case,[26] and ITO(111) in the rest. These hafnia films crystallize totally or partially in the orthorhombic polymorph. The maximum values of remanent polarization are typically in the range of 5–15 $\mu C\ cm^{-2}$, and slightly higher in Ce-doped HfO_2[39] and Y-doped $Hf_{1-x}Zr_xO_2$.[37,38]

The literature reviewed in the previous paragraphs shows that the deposition of an intermediate conducting layer with a non-fluorite crystal structure, which is needed to configure a plane capacitor in the out-of-plane direction, has a detrimental effect on the crystal quality of the growing film. It thus alters the surface energy balance, crystallographic relationships, and epitaxial strain, and hinders the study of the intrinsic effect of the substrate on the stabilization of a particular phase. In an attempt to overcome this limitation, we showed in a previous work that epitaxial $Hf_{0.5}Zr_{0.5}O_2$ can be deposited directly on (001)-oriented YSZ substrates.[40] However, those films had monoclinic structures and were not ferroelectric. We also proved recently that 7 nm-thick $Hf_{0.5}Zr_{0.5}O_2$ films grown on Al_2O_3(0001) without any conducting buffer layer are pyroelectric, that is, non-centrosymmetric and compatible with ferroelectricity.[41] Those samples consisted of few-nanometer-wide grains epitaxially oriented with respect to the substrate's out-of-plane direction but with some degree of mosaic spread in their in-plane orientations. Other authors have also explored the growth of hafnia-based films on bare substrates. Rhombohedral $Hf_{0.5}Zr_{0.5}O_2$ was deposited directly on Si(001) by Nukala et al.[42] and on ZnO(0001) by Zheng et al.[43] Regarding YSZ(111) substrates, epitaxial films of $Hf_{1-y}Y_yO_2$[31] and $Hf_{1-x}Zr_xO_2$[29] deposited directly on them showed orthorhombic structure in a narrow range of film thickness, composition and growth parameters. In both works, the insertion of an ITO intermediate conducting layer deteriorated the crystal quality of the hafnia films, which presented a fraction of non-orthorhombic phases.

Here we demonstrate that high-quality single-phase epitaxial films of $Hf_{0.5}Zr_{0.5}O_2$ (herein denoted HZO) with 7 nm thickness having either monoclinic or orthorhombic structure can be

M. Varela
Departament de Física Aplicada
Universitat de Barcelona
Barcelona 08028, Spain
C. Magén, P. A. Algarabel
Departamento de Física de la Materia Condensada
Universidad de Zaragoza
Zaragoza 50009, Spain
J. A. Pardo
Laboratorio de Microscopías Avanzadas
Universidad de Zaragoza
Zaragoza 50018, Spain

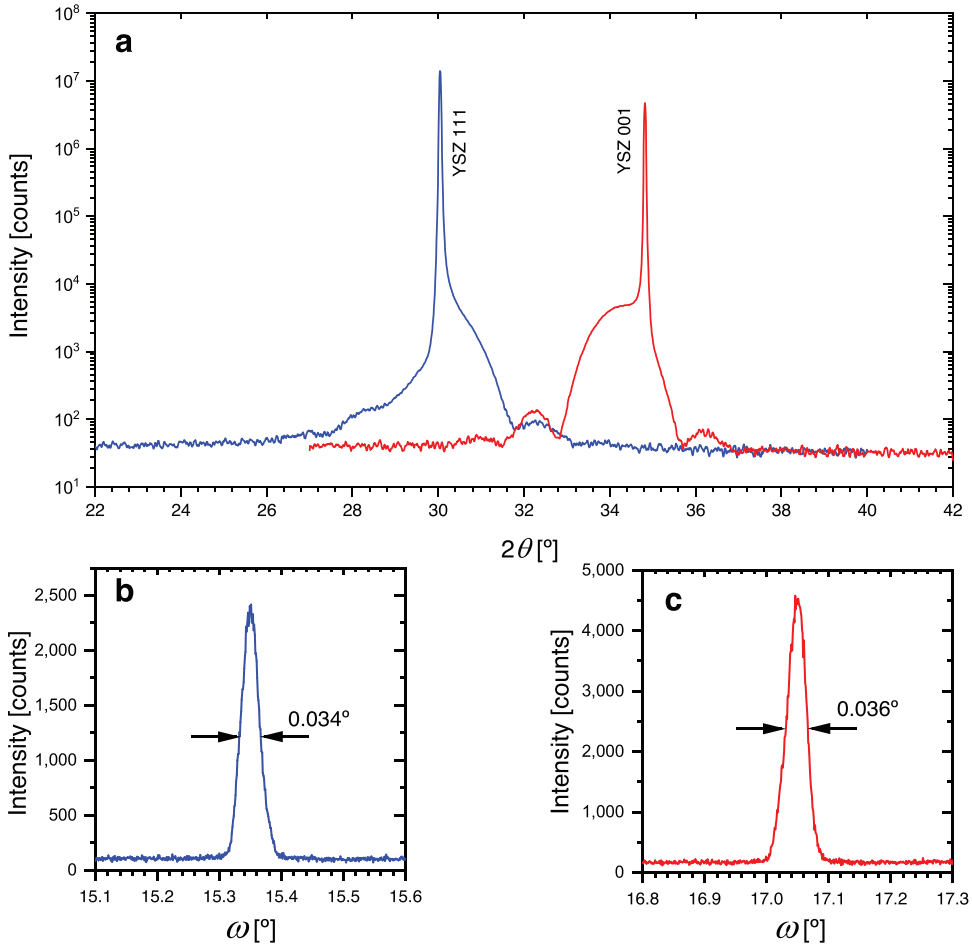

Figure 1. Crystal structure of the 7 nm-thick $Hf_{0.5}Zr_{0.5}O_2$ films deposited simultaneously on YSZ substrates with two different orientations, demonstrating that epitaxial growth is an effective polymorph-selective method. a) $\theta/2\theta$ X-ray diffraction scans, confirming that the samples show a monoclinic structure for YSZ(001) substrate (red line), while a non-monoclinic polymorph emerges on YSZ(111) (blue line). Rocking curves (insets) measured in the previous films at b) $2\theta = 30.7°$ for the YSZ(111) substrate, and c) $2\theta = 34.1°$ for YSZ(001). The values of the full width at half-maximum in these rocking curves indicated in the insets confirm the high crystal quality of these epitaxial films.

grown directly on single-crystal YSZ substrates by selecting their crystallographic orientation. In the case of YSZ(111), orthorhombic films are obtained, as proved by X-ray diffraction and transmission electron microscopy. Additionally, an original strategy that takes advantage of the thermally-stimulated ionic conduction of the HZO/YSZ system and blocking characteristics of the Au/HZO interface is demonstrated for the electrical characterization of the films. In this way, out-of-plane ferroelectric switching is unambiguously proved.

2. Results and Discussion

Symmetric $\theta/2\theta$ X-ray diffractograms measured in both 7 nm-thick films around the 001 and 111 substrate reflections, respectively, are shown in **Figure 1a**.

The sample grown on YSZ(001) presents only a well-defined peak at $2\theta \approx 34.2°$, visible as an intense shoulder on the left side of the narrow peak of the substrate at $2\theta = 34.8°$. It corresponds to the 002 reflection of the equilibrium, monoclinic $P2_1/c$ polymorph of HZO, which is not ferroelectric, in agreement with previous results.[40] However, it is absent in the film grown on YSZ(111). Instead, a non-monoclinic phase emerges in this case, as indicated by the one reflection at $2\theta \approx 30.5°$ (shoulder on the right of the strong 111 peak of YSZ substrate). The crystallite size estimated from this reflection using Scherrer's equation in the film on YSZ(001) was 7.3 ± 0.3 nm, which is very close to the thickness of HZO. A similar calculation could not be done in the sample on YSZ(111) because the peak is almost superimposed to the reflection of the substrate. In addition, in each film, the presence of Von Laue oscillations at both sides of the main reflection demonstrates the crystal coherence along its whole thickness. The angular distance (T) between consecutive minima of these fringes is given by $T = \lambda/(t \times \cos\theta_B)$, being λ the wavelength of the X-ray radiation used, $2\theta_B$ the Bragg angle of the film reflection, and t the film thickness.[44] Using the t value 6.9 ± 0.1 nm measured by XRR gives $T = (1.33 \pm 0.03)°$, in agreement with Figure 1a. This result confirms that the maxima observed at both sides of the main peak are indeed finite-size oscillations, and do not correspond to different phases of HZO. No other peak was detected in broader scans, proving that no other polymorph or

Table 1. . Full width at half-maximum (FWHM) of the rocking curves in hafnia-related epitaxial films reported in several publications. This value is a measure of the film's crystal quality. STO stands for $SrTiO_3$, and LSMO for $(La,Sr)MnO_3$.

Reference	Substrate and orientation	Film composition	Thickness	Bottom electrode	Reflection	FWHM
Wang et al.[46]	STO(001)	$Hf_{0.5}Zr_{0.5}O_2$	5 nm	LSMO	111	0.10°
Wang et al.[46]	STO(001)	$Hf_{0.5}Zr_{0.5}O_2$	9 nm	LSMO	111	0.14°
Wang et al.[46]	STO(001)	$Hf_{0.5}Zr_{0.5}O_2$	15 nm	LSMO	111	2.01°
Yun et al.[47]	STO(001)	$Hf_{0.95}Y_{0.05}O_2$	10 nm	LSMO	111	0.1° and 1° (bimodal)
Bégon-Lours et al.[24]	Si(111)	$Hf_{0.5}Zr_{0.5}O_2$	5.8 nm	GaN(0001)	111	0.26°
Shimizu et al.[31]	YSZ(111)	Cubic or tetragonal $Hf_{0.92}Y_{0.08}O_{2-\delta}$	–	No	222	0.058°
Katayama et al.[48]	YSZ(001)	$Hf_{0.93}Y_{0.07}O_{2-\delta}$	9 nm	No	400	0.12°
Katayama et al.[48]	YSZ(001)	$Hf_{0.93}Y_{0.07}O_{2-\delta}$	9 nm	ITO	400	0.52°
This work	YSZ(001)	$Hf_{0.5}Zr_{0.5}O_2$	7 nm	No	002	0.036°
This work	YSZ(111)	$Hf_{0.5}Zr_{0.5}O_2$	7 nm	No	111	0.034°

orientation is present. The reflection of the film grown on YSZ(111) at $2\theta = 30.5°$ can be indexed as 111 of cubic *Fm*-3*m*, rhombohedral *R*3 or *R*3*m*, or orthorhombic $Pca2_1$ phase, and also as 101 of the $P4_2/nmc$ tetragonal space group. Given that the films were deposited simultaneously, this figure shows the important role played by the substrate orientation to stabilize a particular phase of epitaxial hafnia. This result confirms recent density-functional theory (DFT) calculations,[45] predicting the selection of a specific polymorph in HfO_2 epitaxial films through the constraints (symmetry and strain) imposed by the substrate. Specifically, the study by Zhu et al. proves that the monoclinic phase has the lowest energy on YSZ(001), while orthorhombic $Pca2_1$ is the most stable polymorph on YSZ(111).

The lateral coherence of these samples was assessed by measuring their rocking curves, that is, fixing the detector in the maximum of the film ($2\theta_B$), and then scanning the tilt angle (ω) around θ_B. The results are shown in Figures 1b,c. The full width at half-maximum (FWHM) of both rocking curves is 0.035 + 0.001°. These very low values, slightly larger than that of the substrate (0.015°), are an indication of low mosaic spread and high crystal quality of the films. To our knowledge, all the values of the width of the rocking curves measured in hafnia-based epitaxial films reported previously,[24,31,46–48] are larger, as summarized in **Table 1**.

Further structural characterization was carried out using HAADF-STEM in cross-sectional specimens of the 7 nm-thick HZO films grown on both YSZ(001) and YSZ(111), illustrated in **Figure 2**. In all cases, the films present coherent epitaxial growth, atomic sharp interfaces with the substrate, and no misfit dislocations or interfacial defects. Figure 2a,c depicts an atomic resolution STEM image and its corresponding fast Fourier transform (FFT) of an HZO grain on YSZ(001). Image analysis and simulations confirm that it belongs to the monoclinic polymorph, oriented along the $[010]_m$ zone axis (the subscript *m* stands for monoclinic). Confirming the XRD observations, it grows epitaxially with the $(001)_m$ planes parallel to the (001) cubic planes of the YSZ substrate. Therefore, the *a* and *b* axes of the monoclinic cell are parallel to the in-plane [100] and [010] cubic directions of the YSZ(001) substrate, in agreement with previous results.[40] On the other hand, YSZ(111)-grown HZO films evidence the presence of the non-equilibrium orthorhombic polymorph. For instance, Figure 2b,d displays the image and FFT of an orthorhombic HZO grain that grows epitaxially with the $(111)_o$ planes parallel to the (111) planes of YSZ (the subscript *o* stands for orthorhombic). This particular grain is oriented along the $[11\text{-}2]_o$ zone axis, with the $[-110]_o$ axis parallel to the [−110] of the YSZ substrate.

The polar axis of the orthorhombic $Pca2_1$ phase is believed to lie along the [001] direction,[49] and thus 111-oriented films are expected to show both in-plane and out-of-plane components of the spontaneous polarization. Although the Au interdigital electrodes (IDEs) configuration allows in principle in-plane ferroelectric switching to be characterized, the 20 µm finger separation, along with coercive fields of the order of 1 MV cm^{-1} made measurements not feasible. Indeed, experiments under the required high voltages ≥ 2 kV resulted in the evaporation of the electrodes.

Therefore, an alternative procedure to obtain out-of-plane ferroelectric characteristics was investigated here. The rationale is to use the thermally-activated ionic conductivity of the HZO/YSZ system to turn the substrate into a buried floating electrode, so that two ultrathin film capacitors in series are defined, on which the occurrence of out-of-plane ferroelectric switching in the HZO film can be studied. This only occurs below a threshold frequency that increases as ionic conductivity does, defined by the time necessary to move the required electric charge to the film/electrode interface, where it is blocked due to the absence of an effective ionic-electronic transference mechanism. Note that Au electrodes are classically considered as blocking ones for the oxygen evolution reaction, and working temperatures ≈800 °C and maximized triple-phase-boundary contacts are required to maintain significant faradaic currents.[50] The conditions to reach the blockage for the specific HZO/YSZ epitaxial system with Au IDEs were determined by impedance spectroscopy. **Figure 3** shows the frequency dependence of the impedance modulus for both films, orthorhombic and monoclinic, along with that of a bare substrate with analogous electrodes, at 185 °C. In the case of the film on YSZ(111), that is the orthorhombic one, the curve shows a distinctive impedance plateau related to the HZO layer ionic conductivity (calculated resistivity ≈ 5×10^5 Ω·cm) at intermediate frequencies (≈10–100 Hz). Below this range, impedance

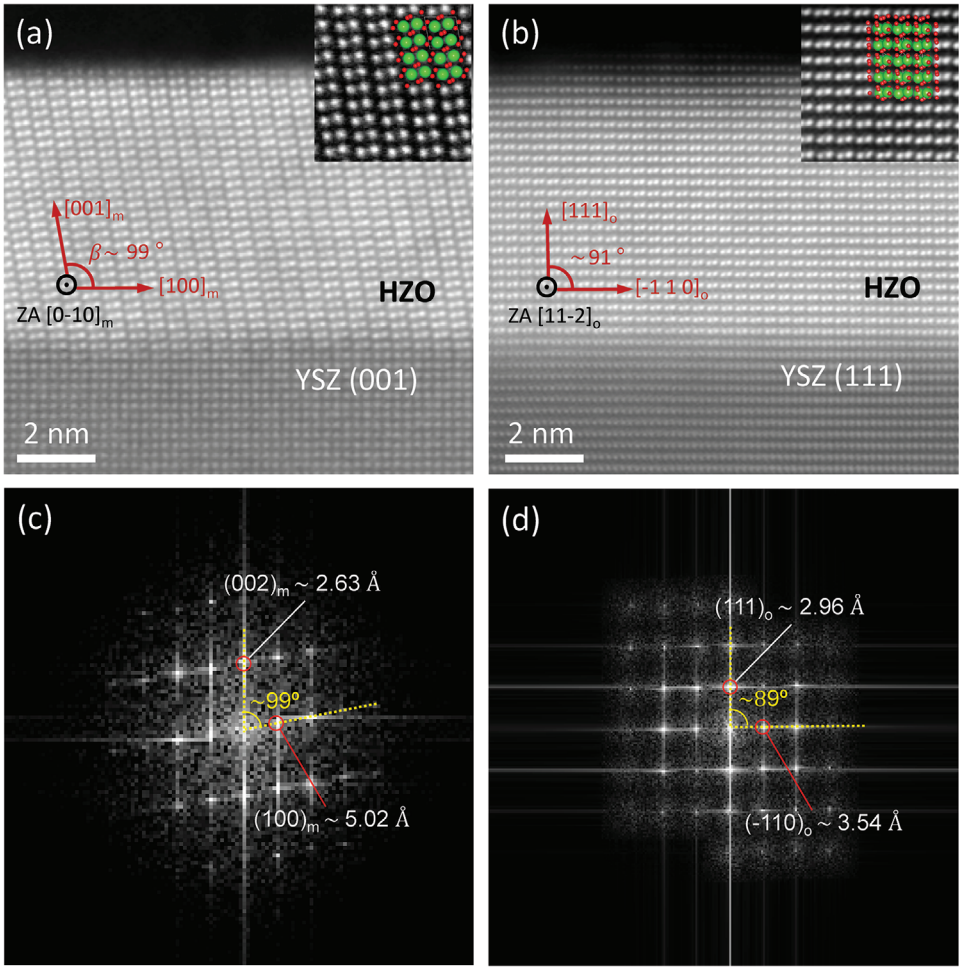

Figure 2. Atomic-resolution cross-sectional HAADF-STEM imaging of the local microstructure of the 7 nm-thick $Hf_{0.5}Zr_{0.5}O_2$ epitaxial films deposited on a) YSZ(001), and b) YSZ(111) substrates, confirming that the sample on YSZ(111) has an orthorhombic crystal structure. Structural models and the crystallographic directions and angles are superimposed on the STEM images. The *m* and *o* subscripts stand for monoclinic and orthorhombic, respectively. *ZA* indicates the zone axis. (c) and (d) show the FFT of (a) and (b), indexed according to the monoclinic and orthorhombic phases, respectively.

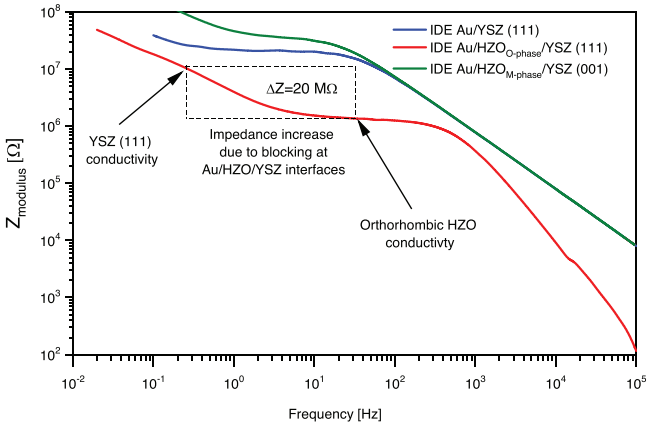

Figure 3. Impedance versus frequency spectra for the HZO/YSZ films with Au IDEs and for a bare YSZ substrate with analogous electrodes. Blockage at the Au/HZO interface in the case of the orthorhombic film, and the associated step-like increase in resistance are highlighted.

increases toward the value of the YSZ substrate in series with the HZO film (calculated resistivity $\approx 10^8$ Ω cm) signaling the blockage at the Au/HZO interfaces. This is complete for 0.01 Hz, at which ionic charge also accumulates at the HZO/YSZ interface creating the required through-thickness electric field for uncovering ferroelectricity. Remarkably, the orthorhombic film presents an ionic conductivity significantly larger than YSZ, contrary to the monoclinic material with a resistivity very close or even higher than that of the substrate. Oxygen vacancies and their electromigration have been reported to play a role in the ferroelectric switching of fluorite-based systems.[51,52]

Ferroelectric characterization was thus accomplished at 185 °C and variable frequency between 1 and 0.01 Hz. Current loops at 0.01 Hz for the monoclinic and orthorhombic films are provided in **Figure** 4a,b, respectively. Note the large difference in current between the two materials, which further indicates the much higher ionic conductivity of the ferroelectric phase. Linear behavior with little hysteresis was found until 2.5 V for both materials, indicating that material systems behave as high-resistance

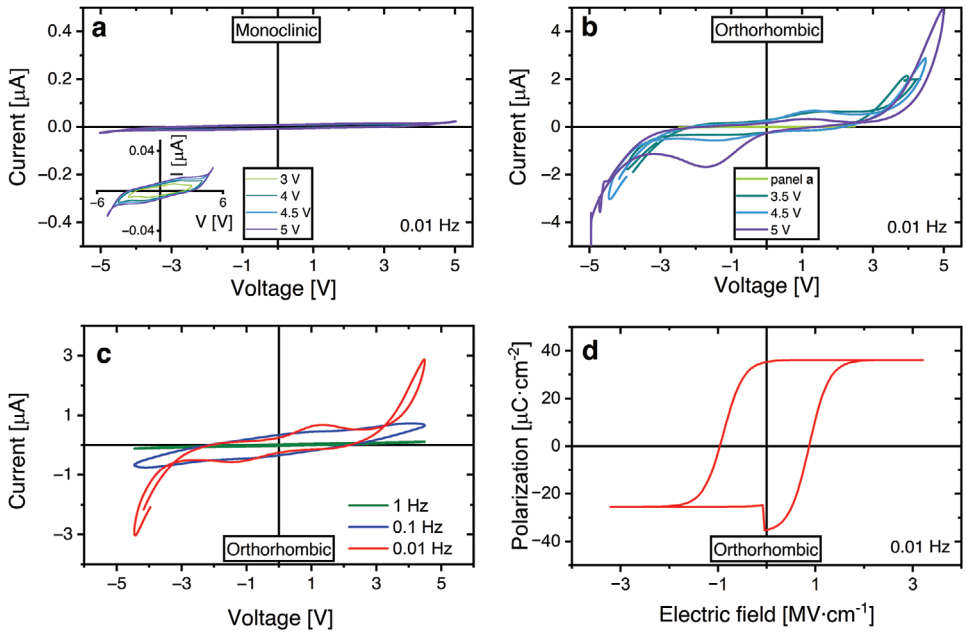

Figure 4. Current–voltage characteristics at 185 °C for a) the monoclinic HZO film on YSZ (001), and b) the orthorhombic HZO film on YSZ (111), measured at 0.01 Hz. c) Current–voltage for the orthorhombic material at decreasing frequencies (1, 0.1, and 0.01 Hz), and d) polarization versus electric field loop extracted from the 0.01 Hz current–voltage curve shown in (c), which confirms the ferroelectric behavior of this film.

elements at low voltages before the ionic charge is blocked at interfaces. In-plane ionic movements dominate the response in this range. Hysteresis appears when voltage is increased for the orthorhombic film, reflecting a capacitive component that signals the charge accumulation at interfaces, followed by the appearance of well-defined switching maxima. Loops at 5 V and decreasing frequency are shown in Figure 4c. An analogous evolution that supports the proposed scenario is found, so that linear behavior with little hysteresis is found at 1 Hz, while hysteresis appears at 0.1 Hz and distinctive ferroelectric switching maxima clearly develop at 0.01 Hz, once charge has time to reach the interfaces. Significant current leakages also appear at high voltages. This requires triggering an unknown redox process, efficient enough to transfer the avalanche-like injected electrons to ions. At this point, the origin of the redox process remains unknown, and its nature and identification will be the subject of subsequent work.

Leakage currents and the capacitive component were evaluated and subtracted from the total response to isolate the ferroelectric contribution, as explained elsewhere.[53] The different components are given in Figure S1 (Supporting Information). Ferroelectric polarization as a function of the electric field is shown in Figure 4d, where the charge was normalized with the area of the fingers of one comb without considering pads (1.5208×10^{-2} cm^2), while the electric field was calculated considering two times the thickness (14 nm). Note that the loop is open at negative polarization because symmetrical current leakages were assumed for the corrections. A remnant polarization $P_r = 35$ μC cm^{-2} and coercive field $E_c = 0.85$ MV cm^{-1} were obtained.

The angle between the [001] polar axis and the out-of-plane [111] direction is $\phi \approx \cos^{-1}[(1/3)^{1/2}]$. Thus, the measured $P_r = 35$ μC cm^{-2} is a projection of the intrinsic remnant polarization, which can be thus estimated as $P_r/\cos(\phi) \approx 61$ μC cm^{-2}. This value would be an overestimation if the relevant electrode area were larger than assumed, that is, if contributions from the pads existed. However, their separation is larger than that of fingers, so these contributions should appear at lower frequencies (they require ionic conduction across the HZO/YSZ system over longer distances). Note that this is the same reason why ferroelectric switching cannot be uncovered using a conventional sandwich structure with electrodes on the HZO film and the opposite surface of the YSZ substrate. The relevant length is the substrate thickness in this case, and even lower frequencies would be necessary. Back to the large remnant polarization, it is worth mentioning that such intrinsic polarization is similar to the value 64 μC cm^{-2} estimated in epitaxial Y-doped HfO_2 films,[47] and higher than the theoretical 51–53 μC cm^{-2} of $Hf_{0.5}Zr_{0.5}O_2$.[54] These polarization values are also quite higher than those reported for polycrystalline hafnia-based films (composed of randomly oriented grains or containing mixtures of polymorphs), which range typically from 10 to 20 μC cm^{-2}.[6,55,56] Remarkably, they are even higher than most values reported for epitaxial $Hf_{0.5}Zr_{0.5}O_2$ films, ranging between 16 and 34 μC cm^{-2}.[19,20] Regarding the coercive field, $E_c \approx 0.85$ MV cm^{-1}, it is within the limits reported in the literature for polycrystalline films (0.75 to 4 MV cm^{-1}),[7,55,56] although slightly smaller than common values for epitaxial films (1.1 to 5 MV cm^{-1}).[19]

Regarding the monoclinic film, no clear ferroelectric switching current maxima comparable to the ones described for the orthorhombic films are observed. When the two orders of magnitude smaller current is amplified (see inset in Figure 4a), broad faint maxima can be observed. They seem to shift toward higher voltages as maximum voltage increases until merging with incipient leakages, which seem to rule out a ferroelectric origin, whose

hypothetical switched polarization otherwise would be extremely low. Maxima might have several origins, even a very limited monoclinic to orthorhombic transition driven by the injection of oxygen vacancies from the YSZ. However, even if appealing and already proposed in the literature,[52] this will be also the subject of future work.

The original approach here demonstrated to study the ferroelectric nature of an all-fluorite epitaxial system makes use of the thermally activated ionic conductivity of the HZO/YSZ system to enable the measurements, and it can be reckoned as an ion-driven electronic effect, namely ferroelectric switching. Several ion-controlled electronic devices, such as memristors or neuromorphic devices have already been proposed and are referred to as iontronics.[57] Although the intrinsically slow response associated with the ion driving precludes memory applications, the ferroelectric all-fluorite system here reported allows poling and thus, might facilitate a range of novel non-switching devices like ion-enabled piezoelectric sensors and actuators.

3. Conclusion

Epitaxial $Hf_{0.5}Zr_{0.5}O_2$ (HZO) films have been grown on electrode-free YSZ by pulsed laser deposition. The films are single-phase and fully-coherent owing to the fluorite-related structure and similar lattice parameters of both the film and the substrate. We have shown that a specific film polymorph can be selected through the choice of the crystallographic orientation of the YSZ substrate. Specifically, the films have the stable, monoclinic crystal structure on YSZ(001) and the metastable orthorhombic on YSZ(111), demonstrating the crucial role of epitaxial stabilization in fluorite-based systems. These experimental results confirm recent density-functional theory calculations by Zhu et al.[45] and pave the way to engineering polymorph selection in hafnia films through the epitaxial growth. Once the HZO films of the orthorhombic phase were deposited directly on YSZ, the ionic conduction of the HZO/YSZ system in the appropriate ranges of temperature and frequency, along with the blocking characteristics of the Au/HZO interface were used for uncovering ferroelectricity. Thanks to this original strategy, we proved the unambiguous out-of-plane ferroelectric switching in the HZO films on YSZ(111). Indeed. This is a new ion-driven electronic effect with the potential to facilitate a range of novel non-switching ferroelectric iontronic devices.

4. Experimental Section

Two films of $Hf_{0.5}Zr_{0.5}O_2$ (HZO) ≈ 7 nm-thick were deposited simultaneously on (001)- and (111)-oriented YSZ single-crystal substrates (Crystal GmbH, with nominally 9.5 mol% Y_2O_3 and lattice parameter $a = 5.15$ Å) by pulsed laser deposition. Figure S2 (Supporting Information) shows the XRR measurements of the two samples and the corresponding fits confirming their thickness value of 6.9 ± 0.1 nm. The growth was carried out at a substrate temperature of 850 °C, a dynamical O_2 pressure of 100 mTorr, and a fluence of 1 J cm^{-2} using a KrF laser operated at a repetition rate of 10 Hz. The films were then cooled down to 20 °C at a rate of 10 °C min^{-1} in the same atmosphere. Other details of the experimental setup were described elsewhere.[40,41] The crystal structure and thickness of the films were studied by high-resolution X-ray diffraction (XRD) and X-ray reflectivity (XRR) using a Bruker D8 Advance diffractometer equipped with parallel-beam optics and monochromated Cu-Kα_1 radiation (wavelength $\lambda = 1.5406$ Å).

The local microstructure of cross-sectional YSZ/HZO specimens was analyzed by high-angle annular dark field (HAADF) imaging in scanning transmission electron microscopy (STEM). Cross-sectional lamellas were fabricated by Ga^+ ion beam milling in a Helios 600 Nanolab. These experiments were carried out in a probe-corrected Thermo Fisher Titan 60–300 microscope equipped with a high-brightness field emission gun (X-FEG) and a CEOS aberration corrector for the condenser system. This microscope was operated at 300 kV to produce a probe size <1 Å. STEM image simulations were carried out with the Dr. Probe software package.[58]

Electrical characterization was performed to study the polar nature of selected films, for that top Au interdigital electrodes (IDEs) with 20 µm separation between the fingers were patterned by optical lithography. First, the complex electrical impedance of the system was studied as a function of temperature and frequency with a Zahner IM6ex Electrochemical Workstation. This aimed at defining the temperature and frequency ranges at which the ionic conductivity of the HZO/YSZ system and its blockage at the Au/HZO interfaces turned the substrate into an effective buried floating electrode. Indeed, above a given temperature and below a certain frequency that depends on the IDEs separation, the system behaves as two capacitors in series and the presence of out-of-plane ferroelectric switching can be studied. A home-built charge-to-voltage converter was used to measure polarization changes at these conditions, while voltage sine waves of increasing amplitude were applied with an HP3325B synthesizer/function generator.

Supporting Information

Supporting Information is available from the Wiley Online Library or from the author.

Acknowledgements

The authors acknowledge financial support by Spanish Agencia Estatal de Investigación through the following grants funded by MCIN/AEI/10.13039/501100011033: PID2019-107338RB-C64, PID2020-112914RB-I00, and PID2021-128281NA-I00. M.A. and R.J. also recognize funding through project TED2021-130871B-C21 / AEI/10.13039/501100011033/ Unión Europea Next Generation EU/PRTR. The authors acknowledge Javier Blasco from INMA-CSIC (Zaragoza, Spain) for the synthesis of the PLD target. Authors acknowledge the use of instrumentation as well as the technical advice provided by the National Facility ELECMI ICTS, node "Laboratorio de Microscopías Avanzadas (LMA)" at the University of Zaragoza.

Conflict of Interest

The authors declare no conflict of interest.

Data Availability Statement

The data that support the findings of this study are available from the corresponding author upon reasonable request.

Keywords

epitaxial growth, ferroelectricity, fluorite structure, hafnia, iontronics

Received: August 3, 2023
Revised: November 8, 2023
Published online:

[1] A. K. Bain, P. Chand, *Ferroelectrics: Principles and Applications*, Wiley-VCH, Weinheim, Germany **2017**.
[2] *Ferroelectric Materials for Energy Applications*, (Eds.: H. Huang, J. F. Scott), Wiley-VCH, Weinheim, Germany **2018**.
[3] T. Mikolajick, U. Schroeder, S. Slesazeck, *IEEE Trans. Electron Devices* **2020**, *67*, 1434.
[4] R. W. Whatmore, Y.-M. You, R.-G. Xiong, C.-B. Eom, *APL Mater.* **2021**, *9*, 070401.
[5] T. S. Böscke, J. Müller, D. Bräuhaus, U. Schröder, U. Böttger, *Appl. Phys. Lett.* **2011**, *99*, 10290.
[6] S. J. Kim, J. Mohan, S. R. Summerfelt, J. Kim, *JOM* **2019**, *71*, 246.
[7] U. Schroeder, M. H. Park, T. Mikolajick, C. S. Hwang, *Nat. Rev. Mater.* **2022**, *7*, 653.
[8] M. Lederer, D. Lehninger, T. Ali, T. Kämpfe, *Phys. Status Solidi RRL* **2022**, *16*, 2200168.
[9] R. Ruh, H. J. Garrett, R. F. Domagala, N. M. Tallan, *J. Am. Ceram. Soc.* **1968**, *51*, 23.
[10] J. E. Lowther, J. K. Dewhurst, J. M. Leger, J. Haines, *Phys. Rev. B* **1999**, *60*, 14485.
[11] J. E. Jaffe, R. A. Bachorz, M. Gutowski, *Phys. Rev. B* **2005**, *72*, 144107.
[12] X. Sang, E. D. Grimley, T. Schenk, U. Schroeder, J. M. Lebeau, *Appl. Phys. Lett.* **2015**, *106*, 162905.
[13] Y. Wei, P. Nukala, M. Salverda, S. Matzen, H. J. Zhao, J. Momand, A. S. Everhardt, G. Agnus, G. R. Blake, P. Lecoeur, B. J. Kooi, J. Iguez, B. Dkhil, B. Noheda, *Nat. Mater.* **2018**, *17*, 1095.
[14] J. P. B. Silva, R. F. Negrea, M. C. Istrate, S. Dutta, H. Aramberri, J. Iguez, F. G. Figueiras, C. Ghica, K. C. Sekhar, A. L. Kholkin, *ACS Appl. Mater. Interfaces* **2021**, *13*, 51383.
[15] A. El Boutaybi, T. Maroutian, L. Largeau, S. Matzen, P. Lecoeur, *Phys. Rev. Materials* **2022**, *6*, 074406.
[16] O. Y.. Gorbenko, S. V. Samoilenkov, I. E. Graboy, A. R. Kaul, *Chem. Mater.* **2002**, *14*, 4026.
[17] R. Batra, T. D. Huan, J. L. Jones, G. Rossetti, R. Ramprasad, *J. Phys. Chem. C* **2017**, *121*, 4139.
[18] D. G. Schlom, L.-Q. Chen, C. J. Fennie, V. Gopalan, D. A. Muller, X. Pan, R. Ramesh, R. Uecker, *MRS Bull.* **2014**, *39*, 118.
[19] I. Fina, F. Sánchez, *ACS Appl. Electron. Mater.* **2021**, *3*, 1530.
[20] J. Cao, S. Shi, Y. Zhu, J. Chen, *Phys. Status Solidi RRL* **2021**, *15*, 2100025.
[21] S. Estandía, N. Dix, J. Gazquez, I. Fina, J. Lyu, M. F. Chisholm, J. Fontcuberta, F. Sánchez, *ACS Appl. Electron. Mater.* **2019**, *1*, 1449.
[22] K. Liu, F. Jin, X. Zhang, K. Liu, Z. Zhang, E. Hua, J. Zhang, H. Ye, G. Gao, C. Ma, L. Wang, W. Wu, *Adv. Funct. Mater.* **2023**, *33*, 2209925.
[23] Y. Zhang, Q. Yang, L. Tao, E. Y. Tsymbal, V. Alexandrov, *Phys. Rev. Applied* **2020**, *14*, 014068.
[24] L. Bégon-Lours, M. Mulder, P. Nukala, S. De Graaf, Y. A. Birkhölzer, B. Kooi, B. Noheda, G. Koster, G. Rijnders, *Phys. Rev. Materials* **2020**, *4*, 043401.
[25] T. Shimizu, K. Katayama, T. Kiguchi, A. Akama, T. J. Konno, H. Funakubo, *Appl. Phys. Lett.* **2015**, *107*, 032910.
[26] T. Li, N. Zhang, Z. Sun, C. Xie, M. Ye, S. Mazumdar, L. Shu, Y. Wang, D. Wang, L. Chen, S. Ke, H. Huang, *J. Mater. Chem. C* **2018**, *6*, 9224.
[27] Z. Zhang, S.-L. Hsu, V. A. Stoica, H. Paik, E. Parsonnet, A. Qualls, J. Wang, L. Xie, M. Kumari, S. Das, Z. Leng, M. Mcbriarty, R. Proksch, A. Gruverman, D. G. Schlom, L.-Q. Chen, S. Salahuddin, L. W. Martin, R. Ramesh, *Adv. Mater.* **2021**, *33*, 2006089.
[28] T. Shimizu, K. Katayama, T. Kiguchi, A. Akama, T. J. Konno, O. Sakata, H. Funakubo, *Sci. Rep.* **2016**, *6*, 32931.
[29] T. Mimura, T. Shimizu, O. Sakata, H. Funakubo, *Phys. Rev. Materials* **2021**, *5*, 114407.
[30] K. Katayama, T. Shimizu, O. Sakata, T. Shiraishi, S. Nakamura, T. Kiguchi, A. Akama, T. J. Konno, H. Uchida, H. Funakubo, *Appl. Phys. Lett.* **2016**, *109*, 112901.
[31] T. Shimizu, K. Katayama, H. Funakubo, *J. Ceram. Soc. Japan* **2018**, *126*, 269.
[32] T. Mimura, T. Shimizu, H. Uchida, O. Sakata, H. Funakubo, *Appl. Phys. Lett.* **2018**, *113*, 102901.
[33] T. Suzuki, T. Shimizu, T. Mimura, H. Uchida, H. Funakubo, *Jpn. J. Appl. Phys.* **2018**, *57*, 11UF15.
[34] T. Mimura, T. Shimizu, T. Kiguchi, A. Akama, T. J. Konno, Y. Katsuya, O. Sakata, H. Funakubo, *Jpn. J. Appl. Phys.* **2019**, *58*, SBBB09.
[35] T. Mimura, T. Shimizu, H. Uchida, H. Funakubo, *Appl. Phys. Lett.* **2020**, *116*, 062901.
[36] R. Shimura, T. Mimura, T. Shimizu, Y. Tanaka, Y. Inoue, H. Funakubo, *J. Ceram. Soc. Japan* **2020**, *128*, 539.
[37] T. Shimizu, Y. Tashiro, T. Mimura, T. Kiguchi, T. Shiraishi, T. J. Konnno, O. Sakata, H. Funakubo, *Phys. Status Solidi RRL* **2021**, *15*, 2000589.
[38] T. Mimura, Y. Tashiro, T. Shimizu, H. Funakubo, *ACS Appl. Electron. Mater.* **2023**, *5*, 1600.
[39] K. Hirai, T. Shiraishi, W. Yamaoka, R. Tsurumaru, Y. Inoue, H. Funakubo, *Jpn. J. Appl. Phys.* **2022**, *61*, SN1019.
[40] L. Torrejón, E. Langenberg, C. Magén, Á. Larrea, J. Blasco, J. Santiso, P. A. Algarabel, J. A. Pardo, *Phys. Rev. Materials* **2018**, *2*, 013401.
[41] E. Barriuso, P. Koutsogiannis, D. Serrate, J. Herrero-Martín, R. Jiménez, C. Magén, M. Algueró, P. A. Algarabel, J. A. Pardo, *Nanomaterials* **2022**, *12*, 1232.
[42] P. Nukala, J. Antoja-Lleonart, Y. Wei, L. Yedra, B. Dkhil, B. Noheda, *ACS Appl. Electron. Mater.* **2019**, *1*, 2585.
[43] M. Zheng, Z. Yin, Y. Cheng, X. Zhang, J. Wu, J. Qi, *Appl. Phys. Lett.* **2021**, *119*, 172904.
[44] A. J. Ying, C. E. Murray, I. C. Noyan, *J. Appl. Crystallogr.* **2009**, *42*, 401.
[45] T. Zhu, S. Deng, S. Liu, *Phys. Rev. B* **2023**, *108*, L060102.
[46] Y. Wang, Q. Wang, J. Zhao, T. Niermann, Y. Liu, L. Dai, K. Zheng, Y. Sun, Y. Zhang, J. Schwarzkopf, T. Schroeder, Z. Jiang, W. Ren, G. Niu, *Appl. Mater. Today* **2022**, *29*, 101587.
[47] Y. Yun, P. Buragohain, M. Li, Z. Ahmadi, Y. Zhang, X. Li, H. Wang, J. Li, P. Lu, L. Tao, H. Wang, J. E. Shield, E. Y. Tsymbal, A. Gruverman, X. Xu, *Nat. Mater.* **2022**, *21*, 903.
[48] K. Katayama, T. Shimizu, O. Sakata, T. Shiraishi, S. Nakamura, T. Kiguchi, A. Akama, T. J. Konno, H. Uchida, H. Funakubo, *J. Appl. Phys.* **2016**, *119*, 134101.
[49] S. Dutta, P. Buragohain, S. Glinsek, C. Richter, H. Aramberri, H. Lu, U. Schroeder, E. Defay, A. Gruverman, J. Iguez, *Nat. Commun.* **2021**, *12*, 7301.
[50] Y. Song, S. Zhou, Q. Dong, Y. Li, X. Zhang, N. Ta, Z. Liu, J. Zhao, F. Yang, G. Wang, X. Bao, *Angew. Chem. Int. Ed. Engl.* **2019**, *58*, 4617.
[51] S. Starschich, S. Menzel, U. Böttger, *Appl. Phys. Lett.* **2016**, *108*, 032903.
[52] P. Nukala, M. Ahmadi, Y. Wei, S. de Graaf, E. Stylianidis, T. Chakrabortty, S. Matzen, H. W. Zandbergen, A. Björling, D. Mannix, D. Carbone, B. Kooi, B. Noheda, *Science* **2021**, *372*, 630 .
[53] R. Jiménez, C. Alemany, M. L. Calzada, A. González, J. Ricote, J. Mendiola, *Appl. Phys. A* **2002**, *75*, 607.
[54] M. Hyuk Park, H. Joon Kim, Y. Jin Kim, T. Moon, C. Seong Hwang, *Appl. Phys. Lett.* **2014**, *104*, 072901.
[55] M. H. Park, D. H. Lee, K. Yang, J.-Y. Park, G. T. Yu, H. W. Park, M. Materano, T. Mittmann, P. D. Lomenzo, T. Mikolajick, U. Schroeder, C. S. Hwang, *J. Mater. Chem. C* **2020**, *8*, 10526.
[56] H. A. Hsain, Y. Lee, M. Materano, T. Mittmann, A. Payne, T. Mikolajick, U. Schroeder, G. N. Parsons, J. L. Jones, *J. Vac. Sci. Technol. A* **2022**, *40*, 010803.
[57] S. Z. Bisri, S. Shimizu, M. Nakano, Y. Iwasa, *Adv. Mater.* **2017**, *29*, 1607054.
[58] J. Barthel, *Ultramicroscopy* **2018**, *193*, 1.